Adsorption of alkali, alkaline-earth, and 3*d* transition metal atoms on silicene

H. Sahin* and F. M. Peeters†

Department of Physics, University of Antwerp, Groenenborgerlaan 171, B-2020 Antwerp, Belgium

(Received 30 August 2012; revised manuscript received 16 December 2012; published 19 February 2013)

The adsorption characteristics of alkali, alkaline-earth, and transition metal adatoms on silicene, a graphene-like monolayer structure of silicon are analyzed by means of first-principles calculations. In contrast to graphene, interaction between the metal atoms and the silicene surface is quite strong due to its highly reactive buckled hexagonal structure. In addition to structural properties, we also calculate the electronic band dispersion, net magnetic moment, charge transfer, work function, and dipole moment of the metal adsorbed silicene sheets. Alkali metals, Li, Na, and K, adsorb to hollow sites without any lattice distortion. As a consequence of the significant charge transfer from alkalis to silicene, metalization of silicene takes place. Trends directly related to atomic size, adsorption height, work function, and dipole moment of the silicene/alkali adatom system are also revealed. We found that the adsorption of alkaline-earth metals on silicene is entirely different from their adsorption on graphene. The adsorption of Be, Mg, and Ca turns silicene into a narrow gap semiconductor. Adsorption characteristics of eight transition metals Ti, V, Cr, Mn, Fe, Co, Mo, and W are also investigated. As a result of their partially occupied *d* orbital, transition metals show diverse structural, electronic, and magnetic properties. Upon the adsorption of transition metals, depending on the adatom type and atomic radius, the system can exhibit metal, half-metal, and semiconducting behavior. For all metal adsorbates, the direction of the charge transfer is from adsorbate to silicene, because of its high surface reactivity. Our results indicate that the reactive crystal structure of silicene provides a rich playground for functionalization at nanoscale.

DOI: 10.1103/PhysRevB.87.085423 PACS number(s): 81.16.Pr, 73.22.Pr, 61.48.−c, 61.72.S−

I. INTRODUCTION

Recent advances in controllable synthesis and characterization of nanoscale materials, have opened up important possibilities for the investigation of ultrathin two-dimensional systems. Chiefly the research efforts directed towards graphene[1,2] have dominated the new era of two-dimensional materials. Many exceptional features of atomically thin graphene layers such as massless Dirac fermions, strength of the lattice structure, high thermal conductivity, and half-integer Hall conductance have been revealed so far.[3–6] In spite of its unique properties, due to the lack of a band gap and its weak light adsorption, graphene research efforts have focused on graphene composites over the past five years. Studies have demonstrated the existence of several chemically converted graphene structures such as grapheneoxide (GO),[7–9] graphane (CH),[10–14] fluorographene (CF),[15–19] and chlorographene (CCl).[20–22] The high-quality insulating behavior, thermal stability, and extraordinary mechanical strength of fluorographene (CF) have inspired intense research on halogenated graphene derivatives.

Unusual properties of graphene promising for a variety of novel applications[23–28] have also triggered significant interest in one or several atom-thick honeycomb structures of binary compounds. Early experimental studies aiming to synthesize and characterize novel monolayer materials have revealed that graphene-like sheets of BN are also stable.[29–31] Though BN has the same planar structure as graphene due to the ionic character of B-N bonds, BN crystal is a wide band gap insulator with an energy gap of 4.6 eV.[32–35] The perfect lattice matching between graphene and BN layers make it possible to construct nanoscale devices.[36] Following the synthesis of hexagonal monolayer of ZnO,[37] the II-VI metal-oxide analog of graphene, it was also predicted that ZnO nanoribbons have ferromagnetic order in their ground state.[38] In addition to these, it was reported that common solvents can be used to exfoliate transition metal dichalcogenides and oxides such as MoS_2, WS_2, $MoSe_2$, $MoTe_2$, $TaSe_2$, $NbSe_2$, $NiTe_2$, Bi_2Te_3, and $NbSe_2$ to obtain single layers.[39–41] Most recently, the possibility of various combinations of MX_2 (M = transition metal, X = chalcogen) type single-layer transition-metal oxides and dichalcogenides, stable even in free-standing form, was also predicted.[42]

The recent synthesis of silicene,[43–45] the silicon analog of graphene has opened a new avenue to nanoscale material research. Though the nanotube[46] and fullerene[47] forms of silicon were synthesized earlier, monolayer silicon was presumed not to exist in a freestanding form. Early theoretical works pointed out that silicene is a semimetal with linearly crossing bands and it has a buckled crystal structure that stems from sp^3 hybridization.[48,49] Similar to graphene, the hexagonal lattice symmetry of silicene exhibits a pair of inequivalent valleys in the vicinity of the vertices of K and K' symmetry points. Moreover, the experimental realization of the transformation of thin films of wurtzite (WZ) materials into the graphene-like thin film structure is another evidence for the existence of monolayer structures of Si and Ge.[50] Recent theoretical studies have revealed several remarkable features of silicene such as a large spin-orbit gap at the Dirac point,[51] experimentally accessible quantum spin Hall effect,[52] transition from a topological insulating phase to a band insulator that can be induced by an electric field[53] and electrically tunable band gap.[54] In addition to unique insulator phases such as quantum spin Hall, quantum anomalous Hall, and band insulator phases, the emergence of a valley-polarized metal phase was also reported very recently.[55] It appears that silicene will be a possible graphene replacement not only due to its graphene-like features but also because of its compatibility to existing silicon-based electronic devices.

In this paper, motivated by the very recent experimental realizations of monolayer silicene,[43–45] we investigate how

alkali, alkaline-earth, and transition metal atoms interact with monolayer freestanding silicene. Details of computational methodology are described in Sec. II. Characteristic properties of monolayer silicene and graphene are compared briefly. Our results on structural and electronic properties of metal adatom adsorbed silicene are presented in Sec. IV. Conclusions and a summary of our results are given in Sec. V.

II. COMPUTATIONAL METHODOLOGY

To investigate the adsorption characteristics of alkali metals and transition metals on a monolayer honeycomb structure of silicone we employ first-principles calculations[56] using the projector augmented wave (PAW) method[57] implemented in VASP code. Electronic exchange-correlation effects are simulated using the spin-polarized local density approximation[58] (LDA). For the plane-wave basis set, the kinetic energy cutoff is taken to be $\hbar^2|\mathbf{k}+\mathbf{G}|^2/2m = 500$ eV. Brillouin zone (BZ) sampling is determined after extensive convergence analysis. In the self-consistent potential, total energy, and binding energy calculations with a $(6\times6\times1)$ supercell of silicene sheet a set of $(5\times5\times1)$ **k**-point sampling is used for BZ integration. For partial occupancies the Gaussian smearing method is used. The convergence criterion of our self-consistent calculations for ionic relaxations is 10^{-5} eV between two consecutive steps. By using the conjugate gradient method, all atomic positions and the size of the unit cell were optimized until the atomic forces were less than 0.05 eV Å^{-1}. Pressures on the lattice unit cell are decreased to values less than 1 kB. Adatom adsorbed silicene monolayers are treated using a supercell geometry, where a minimum of 15 Å vacuum spacing is kept between the adjacent silicene layers. Diffusion pathways of adatoms are calculated for ten different adsorption points on $(4\times4\times1)$ silicene supercell.

The cohesive energy of silicene (also for graphene) per unit cell relative to free Si atom, given in Table I, is obtained from $E_{\rm coh} = 2E_T^{\rm Si} - E_T^{\rm Silicene}$, where $E_T^{\rm Si}$ is the total energy of single free Si and $E_T^{\rm Silicene}$ is the total energy of silicene. Here, the total energies of single atoms are calculated by considering their magnetic ground state. As for the adsorption energy of a metal adatom, one can use the formula $E_{\rm Ads} = E_T^{\rm Ad} + E_T^{\rm Silicene} - E_T^{\rm Silicene+Ad}$ where $E_T^{\rm Silicene}$, $E_T^{\rm Ad}$, and $E_T^{\rm Silicene+Ad}$ are the total energies of the $(6\times6\times1)$ supercell of silicene, isolated single adatom, and silicene + adatom system, respectively.

Most of the adatom adsorption results in a net electrical-dipole moment perpendicular to the plane. Therefore the ground-state electronic structure, magnetic state, and work function are calculated by applying a dipole correction[59] to eliminate the artificial electrostatic field between the periodic supercells. To obtain continuous density of states curves and to determine the energy band gap (E_g), smearing with 0.2 and 0.001 eV is used, respectively. For the charge transfer analysis, the effective charge on the atoms is obtained by the Bader method.[60]

III. SILICENE

Though crystalline silicon has the diamond structure and no layered form exists in nature, very recent experimental studies have reported the successful synthesis of a monolayer of silicon, called silicene, by the application of various deposition techniques. Similar to graphene, silicene can be viewed as a bipartite lattice composed of two interpenetrating triangular sublattices of silicon atoms. Since π bonds between silicon atoms are weaker than in the case of the carbon atoms, planarity is destabilized and therefore silicone atoms are buckled in a silicene crystal. As shown in Fig. 1(b), the buckling (perpendicular distance between these two Si planes) is 0.49 Å. Upon the formation of sp^3 bonded honeycomb lattice, the covalent bond length of Si-Si is 2.25 Å.

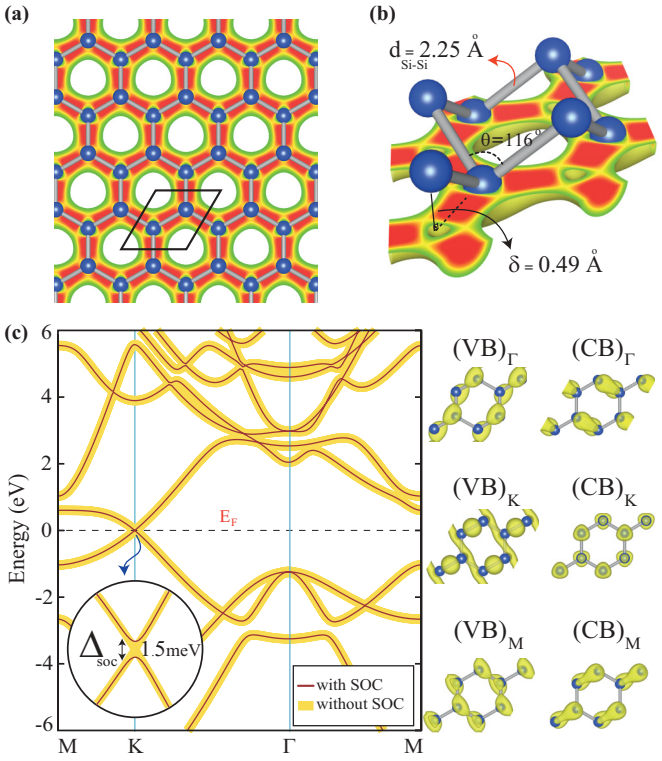

FIG. 1. (Color online) (a) Top view of the honeycomb lattice of silicene and its unit cell shown by a black parallelogram. (b) Tilted view of the 2×2 supercell of silicene. Structural parameters: buckling δ, Si-Si-Si angle, and Si-Si distance are indicated. (c) Electronic band dispersion of silicene (with and without SOC) and band decomposed charge densities of VB and CB at Γ, M, and K symmetry points.

Two-dimensional silicene sheet is a semimetal because the valence and conduction bands touch at the Fermi level. It was predicted earlier that similar to graphene, silicene has also linearly crossing bands at the K (and K') symmetry points and charge carriers in graphene behave like relativistic particles with a conical energy spectrum with Fermi velocity $V_F \cong 10^6$ m s^{-1} like in graphene.[48,49] In Fig. 1(c), the electronic band structure of perfect silicene is presented. Linear π and π^* bands that cross at the K symmetry point are responsible for the existence of massless Dirac fermions in silicene. Due to the degeneracy of the valence band (VB) maxima and the conduction band (CB) minima at the K point, the corresponding states have the same ionization potential and electron affinity. Therefore one can expect the observation of similar unique properties of graphene in silicene. The calculated energy band gaps at M and Γ symmetry points are 1.64 and 3.29 eV, respectively. At the Γ point, the degenerate

TABLE I. Calculated values for graphene, and silicene. These are lattice constant (a), Si-Si (or C-C) bond distance (d), thickness of the layer (t), work function (Φ), cohesive energy per unit cell ($E_{\rm coh}$), in-plane stiffness (C), and optical phonon modes at the Γ point.

Material	a Å	d Å	δ Å	θ rad	Φ eV	$E_{\rm coh}$ eV	C J/m^2	Phonons cm^{-1}
Graphene	2.46	1.42	. . .	120	4.49	17.87	335[a]	900–1600
Silicene	3.83	2.25	0.49	116	4.77	9.07	63[b]	150–580[c]

[a]Reference 19.
[b]Reference 62.
[c]Reference 49.

VB is composed of p_x and p_y orbitals, while the CB is formed by the hybridization of s and p_z orbitals.

In Fig. 1(c), we also present the electronic band dispersion taking into account spin-orbit coupling (SOC). Though clearly the inclusion of spin-orbit interaction does not result in a visible change in band dispersion, a band gap of $\Delta = 1.5$ meV appears at the K point. Due to its buckled structure, silicene has a larger SO-induced gap than graphene, which is of the order of 10^{-3} meV.[61] The calculated band structure and band gap opening (Δ) with SOC is in good agreement with recently reported studies.[51,52,55]

In Table I, we also compare structural, electronic, and vibrational properties of graphene and silicene. It appears that in contrast to the general trend, the larger the atomic radius, the smaller the work function, silicene's work function is 4.77 eV, while for graphene it is 4.49 eV. The calculated values of in-plane stiffness[62] and cohesive energy indicates that silicene is a stable but less stiffer material as compared to graphene. Similar to graphene's out-of-plane optical (ZO) phonon mode at 900 cm^{-1}, silicene has a ZO mode at 150 cm^{-1}. The eigenfrequencies of the LO and TO modes are degenerate at the Γ symmetry point and are found to be 580 cm^{-1}, which is almost three times smaller than graphene's LO (and TO) modes.

IV. RESULTS: ADSORPTION OF METAL ATOMS

As shown in Fig. 2, regarding the interaction of silicene surface with adsorbates, four different adsorption positions can be considered, i.e., above the center of hexagonal silicon rings (hollow site), on top of the upper silicon atoms (top site), on top of the lower silicon atoms (valley site), on top of the Si-Si bond (bridge site). Considering the monolayer hexagonal lattice structure of silicene, it is reasonable to expect the relaxation of foreign atoms to one of these adsorption sites.

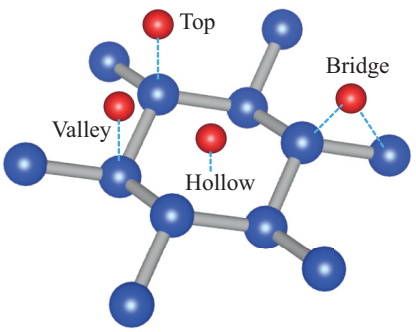

FIG. 2. (Color online) Preferable adsorption sites, hollow, top, hill, and bridge, on a silicene lattice.

A. Bonding geometry and migration barriers

We first investigate the adsorption characteristics of alkali adatoms Li, Na, and K on silicene. The alkali metals are highly reactive metals and their chemical activity increases from Li to Fr. Characteristic bonding geometry of alkali atoms is depicted in Fig. 3. Upon full geometry optimization, all alkali atoms Li, Na, and K, favor bonding on the hollow site of the silicene layer. The adsorption of alkali atoms does not yield any significant distortion or stress on the silicene lattice. The valley site on the low-lying silicon atoms is the next favorable site. Though the top and valley site adsorptions are also possible, bridge site adsorption of alkalis is not possible on a silicene lattice. Therefore the bridge site adsorption is a kind of transition state between top and valley

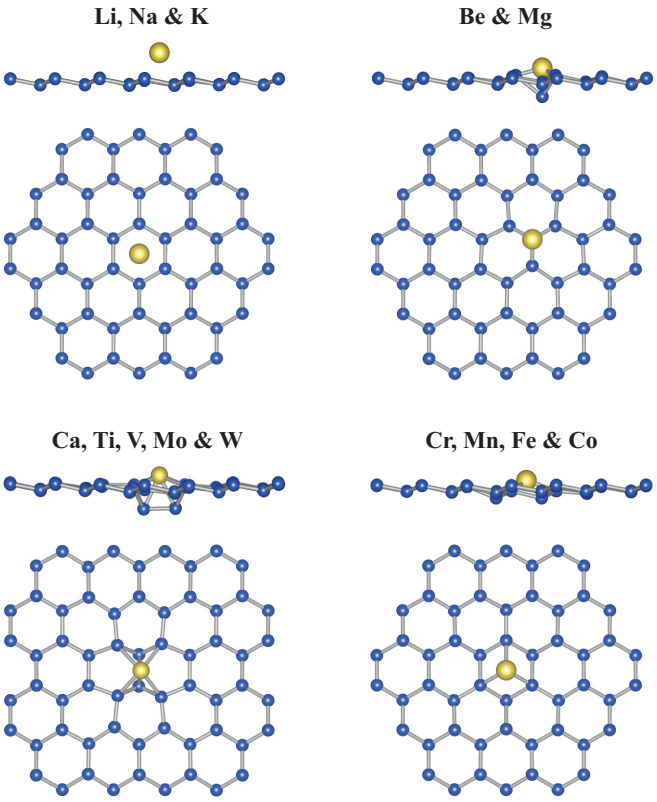

FIG. 3. (Color online) Side and top view for characteristic adsorption geometries for alkali, alkaline-earth, and transition metal atoms.

TABLE II. Calculated values for adatom adsorption on (6×6×1) silicene; relaxation sites hollow (H), bridge (B), valley (V) or top (T), adatom height (h), adsorption energy of adatom ($E_{\rm Ads}$), total magnetic moment of the system ($\mu_{\rm tot}$) in units of Bohr magneton (μ_B), energy band gap (E_g), dipole moment (**p**), Bader charge transferred from adatom to silicene ($\rho_{\rm ad}$), and the work function of the optimized structure (Φ). Metallic and half-metallic structures are denoted as **m** and **hm**, respectively.

	Site	h (Å)	$E_{\rm Ads}$ (eV)	$\mu_{\rm iso}$ (μ_B)	$\mu_{\rm tot}$ (μ_B)	E_g (eV)	**p** (eÅ)	$\rho_{\rm ad}$ (e)	Φ (eV)
Li	**H**	1.69	2.40	1.0	0.0	**m**	0.30	0.8	4.39
Na	**H**	2.19	1.85	1.0	0.0	**m**	0.60	0.8	4.25
K	**H**	2.70	2.11	1.0	0.0	**m**	0.94	0.8	4.09
Be	**V**	0.78	2.87	0.0	0.0	0.39	0.00	1.3	4.68
Mg	**V**	1.98	1.22	0.0	0.0	0.48	0.31	1.0	4.81
Ca	**B**	1.49	2.68	0.0	0.0	0.17	0.62	1.3	4.47
Ti	**B**	0.77	4.89	4.0	2.0	**hm**	0.29	0.9	4.77
V	**B**	0.62	4.32	5.0	2.7	0.06	0.18	0.7	4.84
Cr	**H**	0.48	3.20	6.0	4.0	**hm**	0.12	0.3	4.65
Mn	**H**	1.04	3.48	5.0	3.0	0.24	0.10	0.4	4.73
Fe	**H**	0.33	4.79	4.0	2.0	0.18	0.00	0.0	4.81
Co	**H**	0.72	5.61	3.0	1.0	**m**	0.00	0.0	5.00
Mo	**B**	0.37	5.46	6.0	0.0	**m**	0.15	0.1	4.97
W	**B**	0.01	7.05	6.0	0.0	0.02	0.04	0.2	4.90

sites. Structural and electronic properties of alkali metals adsorbed on silicene layer are also presented in Table II. Here the height of adatoms is calculated as the difference between the average coordinates of neighboring Si atoms and the adsorbate. The distance between the adatom and silicene surface monotonically increases with increasing atomic size. However, fully conforming to graphene,[63] there is no clear trend in the adsorption energies. While adsorption energies of Li, Na, and K on graphene were calculated to be 1.1, 0.5, and 0.8 eV, respectively, their binding to silicene lattice is more than twice stronger, i.e., 2.4, 1.9, and 2.1 eV, respectively. The nature of the alkali-silicene bond will be discussed in the next section.

Possible diffusion pathways of the adsorbate atoms on silicene lattice can also be deduced from the energy barrier between hollow, valley, top, and bridge sites. In Fig. 4, we present the energetics of different adsorption sites. For alkali atoms, shown in Fig. 4(a) it appears that the most likely migration path between subsequent hollow sites passes thorough the nearest valley sites. It is also seen that the energy difference between hollow and valley sites becomes smaller for larger atoms and therefore the diffusion of larger alkali atoms is relatively easier. Though alkali atoms strongly bind to the silicene surface, at high temperatures, they may diffuse along hollow and valley sites when they overcome the energy barrier of 140–280 meV.

Alkaline-earth metals are the elements of the periodic table having two valence electrons in their outermost orbital. Compared to alkalis, alkaline-earth metals have smaller atomic size, higher melting point, higher ionization energy and larger effective charge. Strong interaction between alkaline-earths and silicon surfaces is well known and have been used for various silicon etching and surface engineering techniques. Therefore one can expect strong bonding of alkaline-earth's to a monolayer silicon surface. Resulting atomic geometries for Be, Mg, and Ca adsorbed on a silicene sheet are depicted in Fig. 3. Unlike alkalis, the hollow site is not the most favorable adsorption site for alkaline-earth metals. Among these, while Be and Mg favor adsorption to a valley site, the Ca adsorbate that has a quite large atomic size (empirically

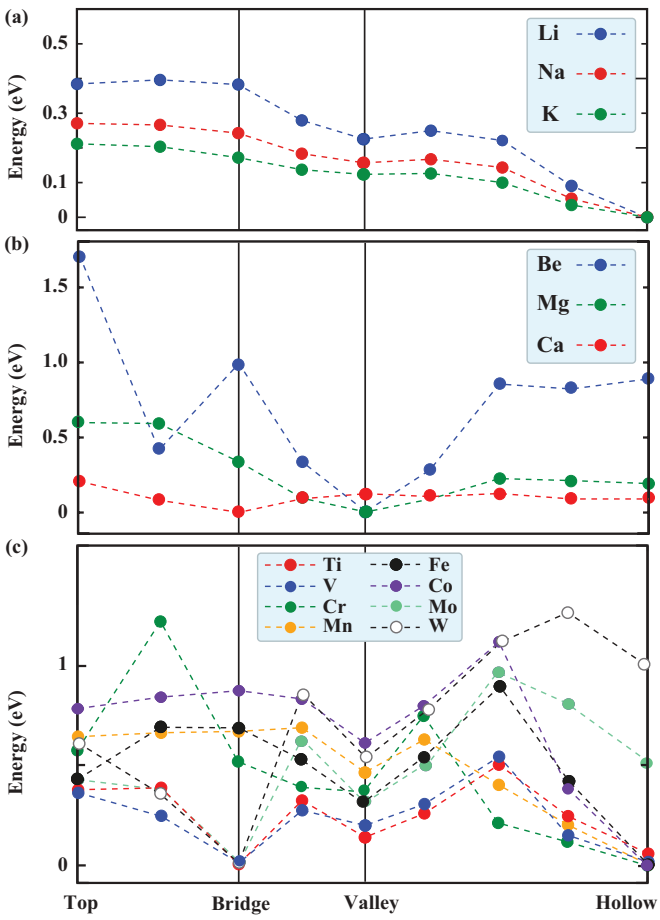

FIG. 4. (Color online) Diffusion pathways and barriers of (a) alkali atoms and (b) 3d, 4d, and 5d transition metals through top, bridge, valley, and hollow sites.

∼1.8 Å) prefers bridge site adsorption. The adsorption energy of alkaline-earth's is slightly higher for alkali metals (except Mg). Similar to the Na adsorbate, a second row element, the adsorption energy has a sharp decrease for the second row alkali element Mg. As shown in Fig. 4(b), the Be atom has to overcome a quite large energy barrier ($\Delta E > 1$ eV) for migration from valley to other adsorption sites. Sudden increases in migration barrier stem from the stretching of silicene lattice by the adsorbate, which is freed only in one direction perpendicular to the surface. At high temperatures, migration of Ca atoms through bridge and hollow sites may take place by overcoming the energy barrier of 125 meV.

We next investigate the adsorption characteristics of eight elements of the 3*d*, 4*d*, and 5*d* transition metal adatoms: Ti, V, Cr, Mn, Fe, Co, Mo, and W. Though the outermost *s* orbitals of the transition metals are completely filled, because of their partially filled inner *d* orbitals, diverse adsorption characteristics for different atoms can be expected. Due to relatively small atomic radius of all transition metals and having more electrons that can participate in the chemical bonding, we can expect stronger binding to the silicene lattice. From Fig. 3, it appears that while the adsorption of alkalis does not cause any significant change in the silicene lattice, transition metals are more likely to disturb the nearest silicon atoms.

Bonding of Ti adatom with 4.89 eV to silicene occurs with a significant lattice distortion whereas the adsorption of Ti occurs on the hollow site of graphene without disturbing the planar lattice structure. As a consequence of bridge-site adsorption of Ti, it binds six nearest Si atoms strongly by pushing the underlying two Si atoms downwards. In order not to exclude possible vacancy formation and adatom-induced fracturing in such Ti-adsorbed silicene lattice, we also examine the stability of the whole structure through molecular dynamics (MD) calculations. *Ab initio* MD calculations show that the adsorbed Ti atom remains bounded and neighboring Si-Si bonds are not broken after ∼1 ps at 300 K. Similar to Ti, a V adatom is adsorbed on a bridge site with 4.32 eV adsorption energy.

Among the 3*d* transition metal adatoms considered here, only Cr, Mn, Fe, and Co, similar to alkalis, are adsorbed on the hollow site. However, differing from alkalis, transition metals have quite strong binding (3.20, 3.48, 4.79, and 5.61 for Cr, Mn, Fe, and Co, respectively) with three uppermost Si atoms. Therefore, instead of being adsorbed on top of a hollow site like alkalis, transition metals are almost confined in the silicene plane. Energetics of transition metal atoms on the most favorable adsorption sites are also listed in Table II.

Note that not only the electronic occupancy but also the atomic radius of the atom is important in determining the final geometry of the adatom on silicene. Since for *d* orbitals having more than half-occupancy the atomic radii are significantly decreased by increasing the number of electrons, starting from Cr all 3*d* transition metals prefer to be relaxed on a hollow site. To see how the atomic radius of transition metal affects the adsorption geometry, we also perform calculations for other group VI elements Mo and W. According to the most recent measurement of Cordero *et al.*,[66] the covalent atomic radii of Cr, Mn, and W are 1.39, 1.54, and 1.62 Å, respectively. In this column of the periodic table, while Cr is adsorbed on a hollow site, bridge site adsorption becomes more preferable for Mo and W due to their larger atomic radii. The effect of the atomic radii can also be seen even in the same row elements: adatoms Ti and V, which have a covalent radius larger than that of Cr, are relaxed to the bridge site. Thus we can infer that only the transition metal adatoms having covalent atomic radii larger than ∼1.50 Å favor bridge site adsorption.

It appears from Fig. 4(c) that the energy barrier between different adsorption sites is relatively large for transition metal atoms. The diffusion barrier between the most favorable site and the less favorable one is ∼0.6 eV. The most likely diffusion path for Ti, V, Mo, and W passes from bridge to hollow sites. However, diffusion of Mn, Cr, Fe, and Co atoms from one hollow site to another one may occur via valley sites.

Furthermore, the effect of spin-orbit interaction on the optimized adsorbate-silicene geometry is examined for adsorption on (6×6×1) silicene supercell. Compared with the optimized geometries obtained excluding SOC, SO-induced change in adatom-silicon bond length is just on the order of 0.001 Å. It is also found that the migration path profile and the most favorable adsorption site do not change when SOC is included. Therefore, due to the negligible effect of spin-orbit interaction on structural properties, in the rest of our study, LDA calculations will be employed.

B. Electronic structure

In this section, we present spin-polarized electronic band dispersion and density of states (DOS) for adatoms adsorbed on the most favorable site on the silicene surface. Since the alkaline-earth and transition metal adsorption significantly disturb the hexagonal lattice symmetry, electronic band dispersion along the high symmetry points (Γ-*M*-*K*-Γ) of perfect silicene may not represent the real electronic properties of the whole structure. Therefore a density of states plot covering large number of *k* points in the BZ is more convenient for a reliable description of the electronic structure.

In Fig. 5, we present electronic band dispersions of alkali metal adsorbed silicene. For the sake of comparison, the band structure of the bare silicene is also included. Here, it is worth

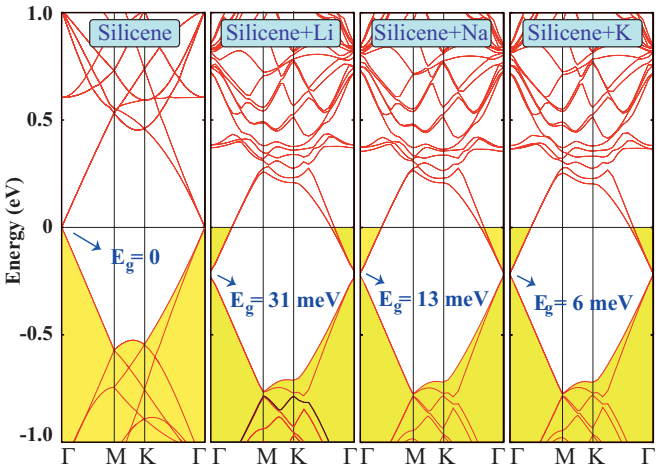

FIG. 5. (Color online) Electronic band structures for perfect, Li, Na, and K adsorbed silicene. Fermi level is set to zero. Occupied bands are filled with yellow color.

to note that the Dirac cone that is located at 2/3 of first BZ is shifted from K to Γ high symmetry point due to band folding of the $(6\times6\times1)$ silicene supercell. Similar shift can be obtained by band folding operations for all $(3n\times3n\times1)$ supercells ($n = 1, 2, \ldots$). As a result of the adsorption of an alkali atom, semimetallic silicene becomes metallic due to the donation of $\sim0.8e$ charge from the alkali atom into the silicene conduction band. Such an attraction of adatom through the hollow site of the silicene surface with a significant charge transfer resembles ionic bonding. Moreover, since the band dispersion of perfect silicene is negligibly disturbed by the alkali adatoms, it seems reasonable to assume that the bonding is of ionic type. Here, in accordance to the charge transfer, the Fermi level (E_F) is shifted by $\sim$0.2 eV. It is seen that all alkali atom adsorption bands formed by the hybridization of adsorbate-s states with the silicene-p states appear in the vicinity of 0.4 eV. Additionally, a small gap opening in the p bands below the Fermi level, which is 6, 13, and 31 meV for Li, Na, and K, respectively, occur at the crossing point.

While each isolated alkali atom has a net initial magnetic moment of $1\mu_B$, up-down spin degeneracy is not broken upon $0.8e$ charge transfer and therefore all the silicene + alkali structures are nonmagnetic metals. However, as a result of the large charge transfer between the alkali atom and silicene, remarkable dipole moment perpendicular to the silicene surface is induced. The calculated value of the dipole moment directed from silicene to the adatom is 0.30, 0.60, and 0.94 e Å for Li, Na and K, respectively. Though the amount of the charge transferred is almost the same for all alkalis, the induced dipole moment is different due to the difference in distance between the adsorbate and the silicene layer. As a consequence of adatom-induced surface charge density redistribution, the work function of the silicene surface is decreased. Therefore the trend of the increase in the dipole moment follows the decrease in work function.

Alkaline-earth metals are highly reactive elements that tend to form various compounds by loosing two outermost shell electrons. Natural silicate and carbonate forms of alkaline-earths are well known. As shown in Table II, Be, Mg, and Ca adsorption yields a gap opening of 0.39, 0.48, and 0.17 eV, respectively. It is also seen from the partial density of states shown in Fig. 6 that the top of the valence band (VB) of Be adsorbed silicene is due to the hybridization of s and p_z orbitals of the nearest silicon atoms and the alkaline-earth metals. However, at the top of the VB, the main contribution comes from Mg-s, Si-s, and Si-p_z hybridization, whereas the p_z orbital of Mg does not mix with surrounding silicon states. The bottom of the conduction band (CB) of both Be and Mg is formed by hybridization of p_{xy} states of adsorbates with p_{xy} and p_z states of silicene. Differing from Be and Mg, the adsorption of Ca on silicene does not yield an appearance of Ca states around E_F. While the states at the VB edge arise mainly from the silicene p_z orbitals, the CB edge is composed of s, p_{xy}, and p_z orbitals of Si.

Since atomic d states of transition metal atoms have comparable energy values to that of their s valence states, the d shell of these atoms is partially filled. The net magnetic moment of isolated transition metals are nonzero and behave like small magnets unless the d shell is completely filled. Though the d-shell electrons are located close to the nucleus,

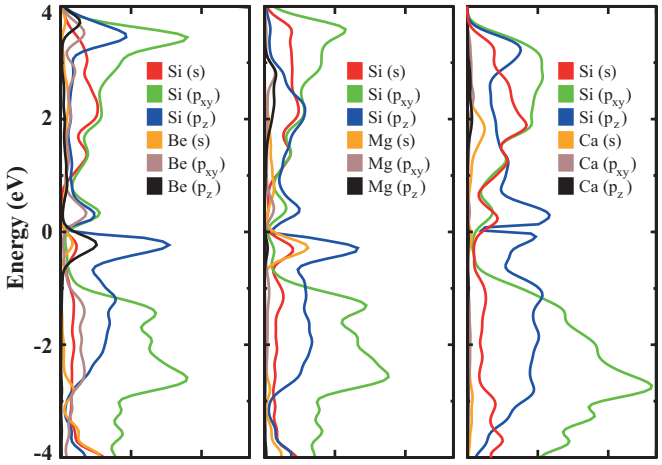

FIG. 6. (Color online) Partial DOS for Be, Mg, and Ca adsorbates and nearest silicon atoms. Fermi level is set to zero. DOS is broadened by Gaussian smearing with 0.2 eV.

like the characteristic core electrons, they can spread out much further like valence electrons. Therefore transition metals with their partially filled d shells are relaxed to different sites on silicene and we can expect diverse electronic properties upon their adsorption. We depict the spin-polarized electronic density of states of those transition metal adsorbed silicenes in Fig 7.

Ti adsorption on silicene has quite different characteristics as compared to other transition metals. Upon the adsorption of a Ti atom that has an initial magnetic moment of $4.0\mu_B$ in its isolated state, on bridge site of silicene, the structure becomes a ferromagnetic metal with a $2.0\mu_B$ net magnetic moment per supercell. Since we use a quite large supercell such that the adatom-adatom interactions are negligible, describing the adatom levels in terms of orbitals, instead of bands, is more appropriate. As a result of the strong bonding, the silicene lattice is significantly distorted, the Ti atom binds to six nearest Si atoms and the degeneracies of the Ti-d states are completely broken. The metallic bands of the structure originate only from the Ti-$d_{x^2-y^2}(\uparrow)$ orbitals, and silicene becomes a half-metal when Ti adatoms are adsorbed.

For the case of V adsorption on silicene, the structure becomes a semiconductor with a 2.7 μ_B net magnetic moment per supercell. It is seen from Fig. 7 that while only V-$d_{xy,yz,xz}(\uparrow)$ states have a significant contribution to VB maximum, the bottom of the CB is derived from Si-$p(\downarrow)$ and V-$d_{xy,yz,xz}(\downarrow)$. The contribution of the other eigenstates at the vicinity of E_F is enhanced just because of the smearing of the DOS plot. Cr adsorption also turns the semimetallic silicene into a half-metallic material with $4\mu_B$ per supercell. The up-spin (minority) bands of the Cr adsorbed silicene are semiconducting with a direct band gap of $\sim$0.4 eV, whereas the down-spin (majority) band shows metallic behavior. The bands in the vicinity of E_F are mainly derived from the hybridization of Cr-$d_{xy,yz,xz}(\downarrow)$ and Cr-$d_{x^2-y^2}(\downarrow)$ orbitals and the Si-$p(\downarrow)$ states. However, differing from Cr, the adsorption of Mo and W that occurs on bridge site results in a nonmagnetic ground state. While Mo-adsorbed silicene becomes metallic due to Mo-$d_{xy,yz,xz}$ states at E_F, W-adsorbed silicene is a

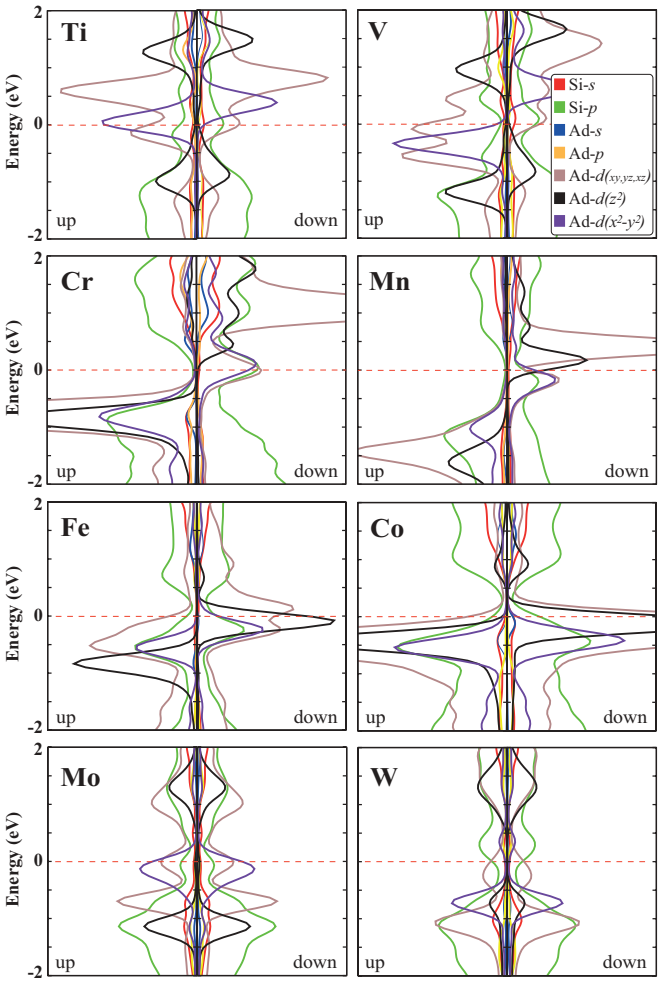

FIG. 7. (Color online) Partial DOS for Ti, V, Cr, and Mn adsorbates and nearest silicon atoms. Fermi level is set to zero. DOS is broadened by Gaussian smearing with 0.2 eV.

nonmagnetic semiconductor with a band gap of 0.02 eV. Note that the half-metallic behavior for Ti- and Cr-decorated silicene can be quite important for potential use in spintronics.

The adsorption of Mn atom in close proximity to the hollow site of buckled hexagonal lattice results in semiconducting behavior with a band gap of 0.24 eV. The degeneracy of ↑ and ↓ spin states is broken due to the existence of a net magnetic moment of $3.0\mu_B$. Since Mn, Fe, and Co atoms have the smallest atomic size of the considered metal atoms here, they are the most closely bonded among all hollow-site adsorbed atoms. The adsorption of both Fe and Co results in a metallic ground state, which originates from the $d_{xy,yz,xz}(\downarrow)$ and $d_{z^2}(\downarrow)$ states at E_F, with 2 and 1 μ_B net magnetic moment, respectively. As a consequence of the small adsorption height, the induced dipole moments are much smaller than those of the alkali adatom adsorbed silicene.

The adsorbate-induced magnetic moments induced in the silicene layer lead to an exchange-splitting especially in d eigenstates. The calculated value of the exchange-splitting is 0.4, 2.0, 2.1, 1.9, 0.5, and 0.4 eV for Ti, V, Cr, Mn, Fe, and Co, respectively. However, bridge-site adsorbed Mo and W adatoms exhibit no splitting due to their nonmagnetic ground state.

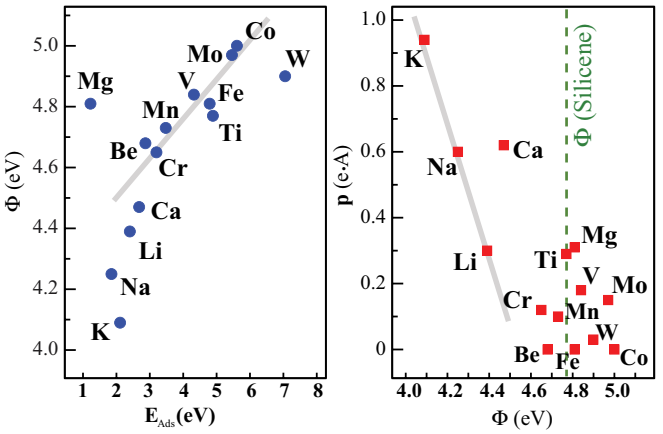

FIG. 8. (Color online) (a) Plot of the adsorption energy E_{Ads} vs the work function Φ and (b) the work function Φ vs dipole moment **p**.

To reveal the correlations between adsorption energy E_{Ads}, work function Φ, and induced dipole moment **p**, we also present Φ-E_{Ads} and **p**-Φ plots as shown in Fig. 8. Note that the adsorption of large transition metals, which occurs with large binding energy, changes the silicene's work function negligibly. Especially for 3d transition metals having more than half-filled d subshells, the larger the adsorption energy the higher the work function. However, it appears that even with a small coverage (1/72) of silicene surface by alkali metals, a significant decrease of the work function can be produced. For alkalis and alkaline-earths, there is almost a linear correlation between E_{Ads} and Φ. Because of the ionic nature of the alkali-silicene bonding, the work function linearly depends on the atomic size and therefore one can expect a significant decrease (>1 eV) in the work function for adsorption of larger alkalis on silicene. It is also seen that, while multivalent adatoms do not follow a particular trend in dipole moment, for alkali atoms, the work function shift exhibits a linear decrease with increasing dipole moment.

V. CONCLUSIONS

In this study, we presented a first-principles investigation of the adsorption characteristics of alkali (Li, Na, and K), alkaline-earth (Be, Mg, and Ca), and transition metals (Ti, V, Cr, Mn, Fe, Co, Mo, and W) on silicene. The investigation of the interaction of silicene with metal atoms has a significant importance because of its fundamental relevance to applications in catalysis, batteries, and nanoelectronics.

We found that silicene has quite different adsorption characteristics as compared to graphene[64,65] because of the diversity of adsorption geometries and its high surface reactivity. As a consequence of its buckled lattice structure, all the metal atoms bind strongly to silicene. While the binding energy of alkali and alkaline-earth metals is 1–3 eV, transition metals have larger binding energies of 3–7 eV. Our diffusion path analysis shows that compared to graphene, the migration of metal atoms on a silicene lattice is more difficult and needs to overcome higher energy barriers. On the other hand, the diffusion of metal atoms Li, Na, K, Mg, and Ca may occur at moderate temperatures. Depending on the adatom

type, semimetallic silicene can show metal, half-metal, or semiconducting behavior. It was also noted that as a result of the high surface reactivity, the direction of the charge transfer is always from the metal adsorbate to silicene. However, the existence of charge donation and the resulting adatom-induced dipole modify the work function of silicene considerably. Especially the linear decrease in Φ for larger alkali adatoms is promising for tunable enhancement of electron and ion emission, which is appealing to silicene-based thermionic converters and cathodes. Our findings also suggest that the half-metallic ferromagnetic nature of Ti- and Cr-decorated silicene has a great potential for silicon-based spintronic device applications. Moreover, the existence of a tunable band-gap opening in silicene by alkaline-earth metal adatoms is highly desirable for its use in nanoscale optoelectronic device applications. The extension of our investigation to a detailed study to include the effect of spin-orbit coupling and of the substrate interactions on the adsorption characteristics of silicene is planned for future studies.

ACKNOWLEDGMENTS

This work was supported by the Flemish Science Foundation (FWO-Vl). Computational resources were provided by TUBITAK ULAKBIM, High Performance and Grid Computing Center (TR-Grid e-Infrastructure). H.S. is supported by a FWO Pegasus Marie Curie Fellowship.

*hasan.sahin@ua.ac.be
†francois.peeters@ua.ac.be

[1] K. S. Novoselov, A. K. Geim, S. V. Morozov, D. Jiang, S. C. Dubonos, I. V. Grigorieva, and A. A. Firsov, Science **306**, 666 (2004).
[2] A. K. Geim and K. S. Novoselov, Nat. Mater. **6**, 183 (2007).
[3] M. I. Katsnelson, K. S. Novoselov, and A. K. Geim, Nat. Phys. **2**, 620 (2006).
[4] K. S. Novoselov, A. K. Geim, S. V. Morozov, D. Jiang, M. I. Katsnelson, I. V. Grigorieva, S. V. Dubonos, and A. A. Firsov, Nature (London) **438**, 197 (2005).
[5] C. Berger, Z. Song, T. Li, X. Li, A. Y. Ogbazghi, R. Feng, Z. Dai, A. N. Marchenkov, E. H. Conrad, P. N. First, and W. A. de Heer, Science **312**, 1191 (2006).
[6] Y. Zhang, Yan-Wen Tan, H. L. Stormer, and P. Kim, Nature (London) **438**, 201 (2005).
[7] D. A. Dikin, S. Stankovich, E. J. Zimney, R. D. Piner, G. H. B. Dommett, G. Evmenenko, S. T. Nguyen, and R. S. Ruoff, Nature (London) **448**, 457 (2007).
[8] G. Eda, G. Fanchini, and M. Chhowalla, Nature Nanotech. **3**, 270 (2008).
[9] J. T. Robinson, F. K. Perkins, E. S. Snow, Z. Wei, and P. E. Sheehan, Nano Lett. **8**, 3137 (2008).
[10] D. C. Elias, R. R. Nair, T. M. G. Mohiuddin, S. V. Morozov, P. Blake, M. P. Halsall, A. C. Ferrari, D. W. Boukhvalov, M. I. Katsnelson, A. K. Geim, and K. S. Novoselov, Science **323**, 610 (2009).
[11] J. O. Sofo, A. S. Chaudhari, and G. D. Barber, Phys. Rev. B **75**, 153401 (2007).
[12] H. Sahin, C. Ataca, and S. Ciraci, Appl. Phys. Lett. **95**, 222510 (2009).
[13] H. Sahin, C. Ataca, and S. Ciraci, Phys. Rev. B **81**, 205417 (2010).
[14] M. Topsakal, S. Cahangirov, and S. Ciraci, Appl. Phys. Lett. **96**, 091912 (2010).
[15] R. R. Nair *et al.*, Small **6**, 2877 (2010).
[16] J. T. Robinson, J. S. Burgess, C. E. Junkermeier, S. C. Badescu, T. L. Reinecke, F. K. Perkins, M. K. Zalalutdniov, J. W. Baldwin, J. C. Culbertson, P. E. Sheehan, and E. S. Snow, Nano Lett. **10**, 3001 (2010).
[17] F. Withers, M. Dubois, and A. K. Savchenko, Phys. Rev. B **82**, 073403 (2010).
[18] O. Leenaerts, H. Peelaers, A. D. Hernandez-Nieves, B. Partoens, and F. M. Peeters, Phys. Rev. B **82**, 195436 (2010).
[19] H. Sahin, M. Topsakal, and S. Ciraci, Phys. Rev. B **83**, 115432 (2011).
[20] B. Li, L. Zhou, D. Wu, H. Peng, K. Yan, Y. Zhou, and Z. Liu, ACS Nano. **5**, 5957 (2011).
[21] H. Sahin and S. Ciraci, J. Phys. Chem. C **116**, 24075 (2012).
[22] M. Ijas, P. Havu, and A. Harju, Phys. Rev. B **85**, 035440 (2012).
[23] C. Ataca, E. Akturk, H. Sahin, and S. Ciraci, J. Appl. Phys. **109**, 013704 (2011).
[24] M. Topsakal, H. Sahin, and S. Ciraci, Phys. Rev. B **85**, 155445 (2012).
[25] H. Sahin and S. Ciraci, Phys. Rev. B **84**, 035452 (2011).
[26] X. Miao, S. Tongay, M. K. Petterson, K. Berke, A. G. Rinzler, B. R. Appleton, and A. F. Hebard, Nano Lett. **12**, 2745 (2012).
[27] S. Tongay, M. Lemaitre, X. Miao, B. Gila, B. R. Appleton, and A. F. Hebard, Phys. Rev. X **2**, 011002 (2012).
[28] S. Tongay, M. Lemaitre, T. Schumann, K. Berke, B. R. Appleton, B. Gila, and A. F. Hebard, Appl. Phys. Lett. **99**, 102102 (2011).
[29] K. S. Novoselov, D. Jiang, F. Schedin, T. Booth, V. V. Khotkevich, S. Morozov, and A. K. Geim, Proc. Natl. Acad. Sci. USA **102**, 10451 (2005)
[30] C. Jin, F. Lin, K. Suenaga, and S. Iijima, Phys. Rev. Lett. **102**, 195505 (2009).
[31] L. Ci, L. Song, C. Jin, D. Jariwala, D. Wu, Y. Li, A. Srivastava, Z. F. Wang, K. Storr, L. Balicas, F. Liu, and P. M. Ajayan, Nat. Mater. **9**, 430 (2010).
[32] Z. Zhang and W. Guo, Phys. Rev. B **77**, 075403 (2008).
[33] Cheol-Hwan Park and Steven G. Louie, Nano Lett. **8**, 2200 (2008).
[34] V. Barone and J. E. Peralta, Nano Lett. **8**, 2210 (2008).
[35] M. Topsakal, E. Akturk, and S. Ciraci, Phys. Rev. B **79**, 115442 (2009).
[36] K. S. Novoselov, Ang. Chem. Int. Ed. **50**, 6986 (2011).
[37] C. Tusche, H. L. Meyerheim, and J. Kirschner, Phys. Rev. Lett. **99**, 026102 (2007).
[38] A. R. Botello-Mendez, F. Lopez-Urias, M. Terrones, and H. Terrones, Nano Lett. **6**, 1562 (2008).
[39] J. N. Coleman *et al.*, Science **331**, 568 (2011).
[40] K. F. Mak, C. Lee, J. Hone, J. Shan, and T. F. Heinz, Phys. Rev. Lett. **105**, 136805 (2010).

[41]Z. Wang, K. Zhao, H. Li, Z. Liu, Z. Shi, J. Lu, K. Suenaga, S. Joung, T. Okazaki, Z. Jin, Z. Gu, Z. Gao, and S. Iilima, J. Mater. Chem. **21**, 171 (2011).
[42]C. Ataca, H. Sahin, and S. Ciraci, J. Phys. Chem. C **116**, 8983 (2012).
[43]P. De Padova, C. Quaresima, C. Ottaviani, P. M. Sheverdyaeva, P. Moras, C. Carbone, D. Topwal, B. Olivieri, A. Kara, H. Oughaddou, B. Aufray, and G. Le Lay, Appl. Phys. Lett. **96**, 261905 (2010).
[44]P. De Padova, C. Quaresima, P. Perfetti, B. Olivieri, B. Leandri, B. Aufray, S. Vizzini, and G. Le Lay, Nano Lett. **8**, 271 (2008).
[45]P. Vogt, P. De Padova, C. Quaresima, J. Avila, E. Frantzeskakis, M. C. Asensio, A. Resta, B. Ealet, and G. Le Lay, Phys. Rev. Lett. **108**, 155501 (2012).
[46]D. F. Perepichka and F. Rosei, Small **2**, 22 (2006).
[47]B. Marsen and K. Sattler, Phys. Rev. B **60**, 11593 (1999).
[48]S. Cahangirov, M. Topsakal, E. Aktürk, H. Sahin, and S. Ciraci, Phys. Rev. Lett. **102**, 236804 (2009).
[49]H. Sahin, S. Cahangirov, M. Topsakal, E. Bekaroglu, E. Aktürk, R. T. Senger, and S. Ciraci, Phys. Rev. B **80**, 155453 (2009).
[50]D. Wu, M. G. Lagally, and F. Liu, Phys. Rev. Lett. **107**, 236101 (2011).
[51]Cheng-Cheng Liu, H. Jiang, and Y. Yao, Phys. Rev. B **84**, 195430 (2011).
[52]Cheng-Cheng Liu, W. Feng, and Y. Yao, Phys. Rev. Lett. **107**, 076802 (2011).
[53]M. Ezawa, New J. Phys. **14**, 033003 (2012).
[54]N. D. Drummond, V. Zolyomi, and V. I. Fal'ko, Phys. Rev. B **85**, 075423 (2012).
[55]M. Ezawa, Phys. Rev. Lett. **109**, 055502 (2012).
[56]G. Kresse and J. Hafner, Phys. Rev. B **47**, 558 (1993); G. Kresse and J. Furthmüller, *ibid*. **54**, 11169 (1996).
[57]P. E. Blochl, Phys. Rev. B **50**, 17953 (1994).
[58]D. M. Ceperley and B. J. Alder, Phys. Rev. Lett. **45**, 566 (1980).
[59]G. Makov and M. C. Payne, Phys. Rev. B **51**, 4014 (1995).
[60]G. Henkelman, A. Arnaldsson, and H. Jonsson, Comput. Mater. Sci. **36**, 254 (2006).
[61]Y. Yao, F. Ye, X. L. Qi, S. C. Zhang, and Z. Fang, Phys. Rev. B **75**, 041401(R) (2007).
[62]R. Qin, C.-H. Wang, W. Zhu, and Y. Zhang, AIP Advances **2**, 022159 (2012)
[63]K. T. Chan, J. B. Neaton, and M. L. Cohen, Phys. Rev. B **77**, 235430 (2008).
[64]T. O. Wehling, M. I. Katsnelson, and A. I. Lichtenstein, Phys. Rev. B **80**, 085428 (2009).
[65]T. O. Wehling, A. I. Lichtenstein, and M. I. Katsnelson, Phys. Rev. B **84**, 235110 (2011).
[66]B. Cordero, V. Gómez, A. E. Platero-Prats, M. Revés, J. Echeverría, E. Cremades, F. Barragán, and S. Alvarez, Dalton Trans. (2008), 2832.